Int. J. Electrochem. Sci., 12 **(2017)** 10015 – 10022, doi: 10.20964/2017.11.44

International Journal of
ELECTROCHEMICAL
SCIENCE
www.electrochemsci.org

Enhanced Energy Density of Supercapacitors Using Hybrid Electrodes Based on Fe_2O_3 and MnO_2 Nanoparticles

Green Kim, Jinhyeon Kang, Geunpyo Choe and Sanggyu Yim[*]

Department of Chemistry, Kookmin University, Seoul, 02707, South Korea
[*]E-mail: sgyim@kookmin.ac.kr

Received: 3 July 2017 / *Accepted:* 5 September 2017 / *Published:* 12 October 2017

A major limitation of transition metal oxide-based electrodes for supercapacitors is their low energy densities. Since the energy density is proportional to the specific capacitance and square of the operating voltage, extending the voltage window of the electrode as well as enhancing contacts with electrolyte is of utmost importance. In this paper, we focus on the hybrid electrode based on Fe_2O_3 and MnO_2 nanoparticles (NPs) which have different redox potential ranges, aiming for the increase of the specific capacitance and operating voltage window simultaneously. The hybrid Fe_2O_3/MnO_2 NPs-based electrode exhibited significantly improved energy density of 12.5 Wh/kg at a power density of 4500 W/g. The energy density of the hybrid electrode is 3.8 times and 1.3 times larger than that of the Fe_2O_3 and MnO_2 single electrode, respectively.

Keywords: supercapacitor, iron oxide, manganese oxide, nanoparticle, hybrid electrode.

1. INTRODUCTION

Electrochemical energy storage is a rapidly growing issue of technology due to the tremendously increasing energy demand for portable electronics, electrical vehicles and cellular devices [1]. Among the various energy storage technologies, supercapacitor has attracted increasing attention owing to its attractive characteristics such as high power density, long cycle life and low equivalent series resistances [2-4]. However, substantial challenges still remain to replace existing market because of its small energy density compared to the secondary batteries. Supercapacitors are generally classified into two types according to the electrode material and energy storing mechanism, electrochemical double layer capacitor (EDLC) and pseudocapacitor [1,3,5]. While the EDLC uses mainly activated carbons, the pseudocapacitor adopts transition metal oxides (TMOs) and conductive polymers as an electrode material. The pseudocapacitor shows higher specific capacitance (C_{sp})

because it uses faradaic redox reactions of the electrode materials, as compared to the EDLC which uses non-faradaic charge storage on the electrode surface [3,6].

Among various TMOs, ruthenium oxide (RuO_2) was most widely studied in an earlier stage because of its superior electrochemical properties such as excellent proton transfer and reversible redox characteristics and hence high C_{sp} values of 900 – 1400 F/g reported [7,8]. However, the practical use of RuO_2 is severely limited by its extraordinarily high price, and hence much cheaper electrode materials such as iron oxide [9,10], copper oxide [11,12], manganese oxide [13,14] and vanadium oxide [15] were recently focused on. However, the electrochemical performance of the electrodes such as specific capacitance was far below their theoretical values and the value of RuO_2, which is mainly attributed to their poor electrical conductivities [16-18]. In this context, various TMO nanostructures were proposed for the efficient ion transport between the electrodes and electrolytes, and consequent increases in C_{sp} value to some extent were reported [19-21]. In spite of the C_{sp} increases, however, the enhancement in the energy density of the electrodes was not apparent, which is probably attributed to the limited redox potential range of the TMOs. The operating voltage determined by the redox potential of the electrode materials has a great impact on the energy density of the supercapacitor cell since the energy density is proportional to the square of the operating voltage [22,23],

$$E = \frac{1}{2} C(\Delta V)^2 \qquad (1)$$

where C is the specific capacitance and ΔV is the potential window.

In this work, we focused on the hybrid electrodes based on two TMO nanoparticles (NPs), Fe_2O_3 NPs and MnO_2 NPs, having different redox potential ranges, in order for increased specific capacitance and voltage window simultaneously, and consequent enhancement in energy density of the electrodes. The faradaic charge storage of Fe_2O_3 in alkaline or neutral media involves the following redox reaction between Fe(III) and Fe(II) oxidation states [24,25],

$$Fe_2^{III}O_3 + 3H_2O + 2e^- \leftrightarrow 2Fe^{II}(OH)_2 + 2OH^- \qquad (2)$$

The Fe_2O_3 electrodes operate over a wide negative voltage window of -1.1 – 0.2 V [16,26,27]. In contrast, the MnO_2 electrodes were reported to operate normally over positive potential window of 0.0 – 1.0 V, involving the intercalation and deintercalation of electrolyte cations (C^+) [14,28].

$$MnO_2 + C^+ + e^- \leftrightarrow MnOOC \qquad (3)$$

The hybrid of these two materials with different operating voltage ranges is therefore expected to exert synergetic effect on the energy density of the electrodes.

2. EXPERIMENTAL

2.1. Fabrication of Fe_2O_3 and MnO_2 nanoparticles

For the synthesis of Fe_2O_3 NPs, commercially available iron(III) nitrate ($Fe(NO_3)_3$, Sigma-Aldrich) (7.5 g) was dissolved in distilled water (200 ml) and vigorously stirred at 100˚C for 2 h. The solution was then cooled down to room temperature. The red precipitate was filtered, washed with

distilled water, and dried under vacuum for 12 h. For the synthesis of MnO_2 NPs, 9.0 g of $KMnO_4$ (Sigma Aldrich) was thoroughly dissolved in distilled water (150 ml) at room temperature. A solution of ascorbic acid (3.0 g) dissolved in distilled water (45 ml) was added slowly into the $KMnO_4$ solution using a syringe pump, followed by additional stirring for 2 h. The brownish precipitate was filtered, washed with distilled water, and dried in an oven at 60˚C for 24 h.

2.2. Fabrication of hybrid Fe_2O_3/MnO_2 electrodes

NPs-deposited electrodes were fabricated by dipping a nickel foam current collector in a slurry containing metal oxide NPs as active material, super-P as conductive additive, and polytetrafluoroethylene (PTFE, Aldrich) as polymeric binder (8:1:1 weight ratio). Loading mass of the active material was approximately 1.0 mg per 1 cm^2 current collector, determined by the microbalance.

2.3. Characterization

The morphology and crystallinity of the Fe_2O_3 and MnO_2 NPs were characterized by field emission scanning electron microscopy (FE-SEM, JEOL JSM-7410F, JEOL Ltd.) and X-ray diffraction (XRD, Rigaku D/Max 2500). The cyclic voltammetry (CV) and galvanostatic charge-discharge (GCD) measurements for the fabricated electrodes were conducted in a 1 M Na_2SO_4 aqueous solution at room temperature using a cyclic voltammeter (ZIVE SP2, WonATech). The measurements were performed in a three-electrode electrochemical cell in which the Fe_2O_3, MnO_2 or Fe_2O_3/MnO_2 electrode was used as a working electrode, a platinum plate was used as a counter electrode, and Ag/AgCl (in 3.0 M KCl) was used as a reference electrode.

3. RESULTS AND DISCUSSION

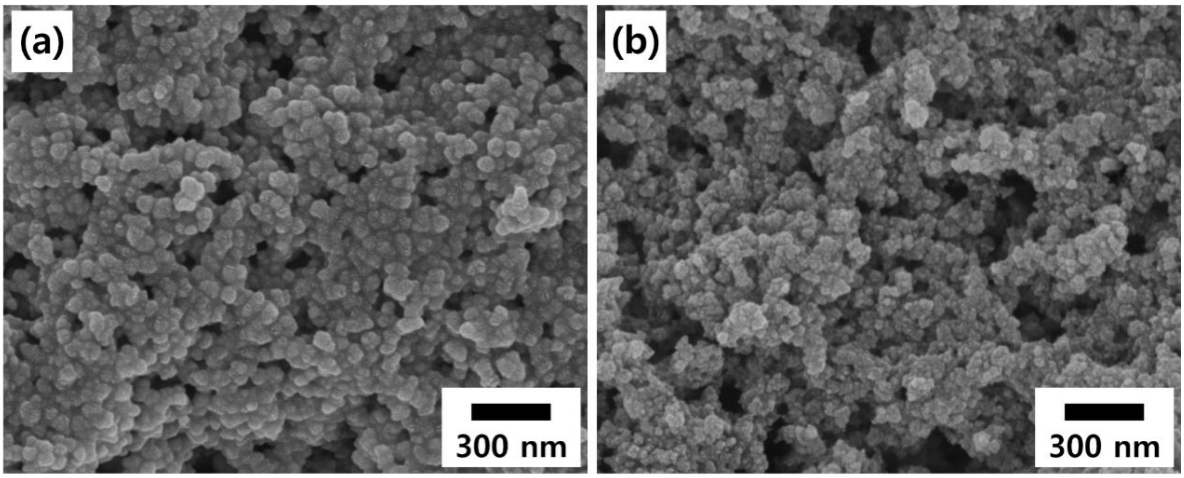

Figure 1. FE-SEM images of synthesized (a) Fe_2O_3 and (b) MnO_2 nanoparticles.

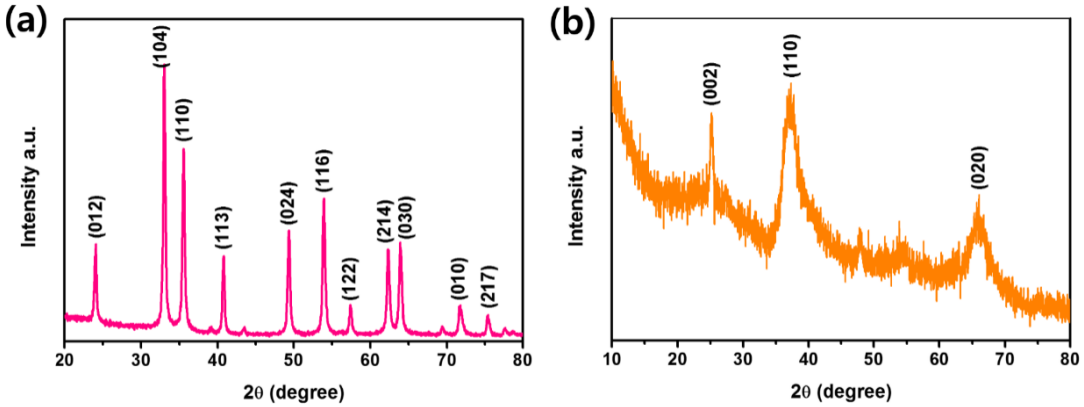

Figure 2. XRD patterns of synthesized (a) Fe_2O_3 and (b) MnO_2 nanoparticles.

Figs. 1(a) and 1(b) show the representative FE-SEM images of synthesized Fe_2O_3 and MnO_2 NPs, respectively. It was observed that both types of nanoparticles were of similar size, approximately 50 nm in diameter. The crystalline phases of the NPs were characterized by XRD, as shown in Fig. 2. The pattern of the Fe_2O_3 NPs (Fig. 2a) exhibits clear and sharp diffractions corresponding to the hematite α-Fe_2O_3 phase (JCPDS 89-0597). The diffraction peaks of MnO_2 NPs (Fig. 2b) can be matched with the birnessite-type MnO_2 (JCPDS 42-1317). Relatively broader pattern indicates the poorer crystalline structure of MnO_2 NPs prepared by reduction of $KMnO_4$ [29]. The XRD of mixed Fe_2O_3/MnO_2 composites showed a pattern that the two diffraction patterns were simply combined.

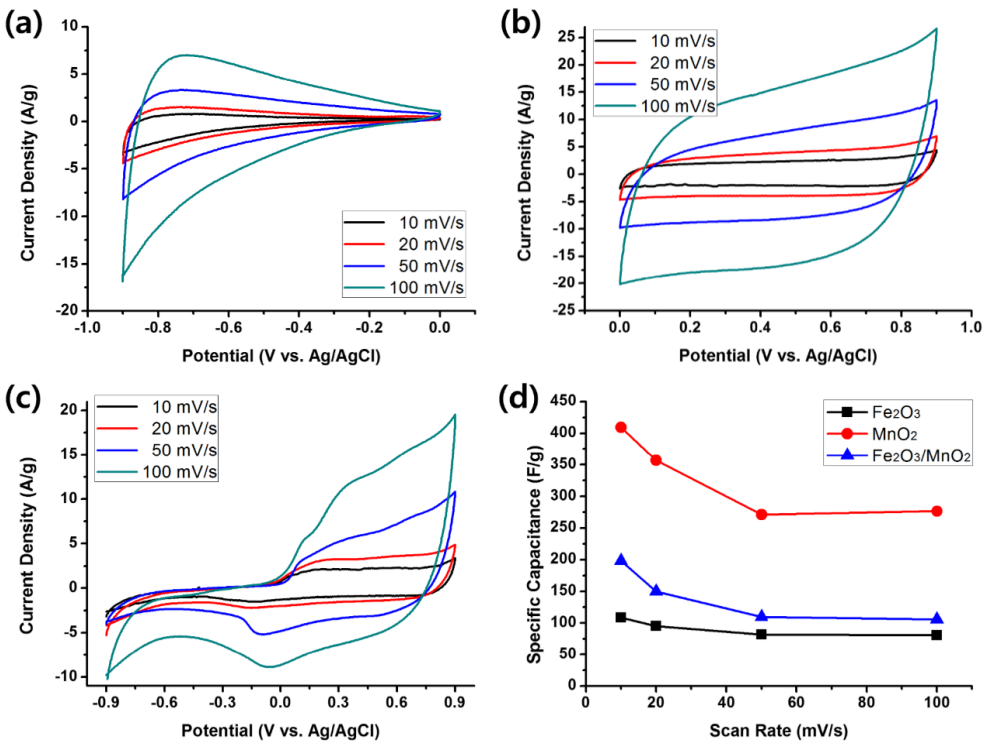

Figure 3. Cyclic voltammograms of the (a) Fe_2O_3 single, (b) MnO_2 single and (c) Fe_2O_3/MnO_2 hybrid electrodes measured at various scan rates. (d) Plots of the C_{sp} values of the electrodes as a function of the number of the scan rate.

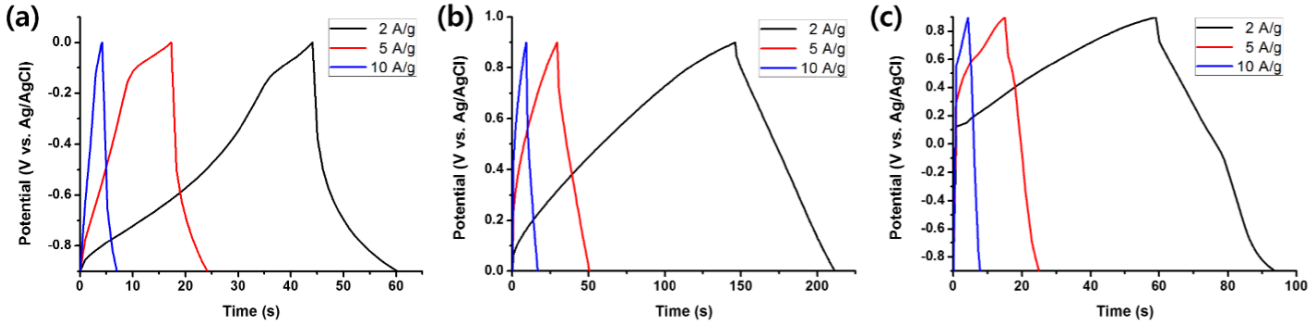

Figure 4. Galvanostatic charge-discharge curves of the (a) Fe_2O_3 single, (b) MnO_2 single and (c) Fe_2O_3/MnO_2 hybrid electrodes measured at various current densities.

The electrochemical properties of Fe_2O_3 single, MnO_2 single and Fe_2O_3/MnO_2 hybrid electrodes were investigated by CV measurements in 1 M Na_2SO_4 aqueous solution, as shown in Fig. 3. Figs. 3(a) and 3(b) show CV curves of the Fe_2O_3 and MnO_2 NPs-based electrodes, respectively, at various scan rates ranging from 10 mV/s to 100 mV/s. While the redox reactions of the Fe_2O_3 electrodes are stable in the negative potential range, -0.9 – 0.0 V, those of the MnO_2 electrodes are stable in the positive potential range, 0.0 – 0.9 V. The specific capacitance, C_{sp}, of the electrodes was calculated by the following equation,

$$C_{sp} = \frac{I}{m(dV/dt)} \qquad (4)$$

where I (A) is the average current, m (g) is the mass of deposited metal oxide NPs and dV/dt (mV/s) is the scan rate [30]. In the case of the Fe_2O_3 electrodes, a maximum C_{sp} value was 108 F/g, measured at the scan rate of 10 mV/s. For the MnO_2 electrodes, however, the maximum C_{sp} value of 409 F/g was obtained at the same measurement condition.

A Fe_2O_3/MnO_2 hybrid electrode was also prepared aiming for wide voltage range and high energy density. A well-mixed slurry consisting of Fe_2O_3 and MnO_2 NPs, super-P, and PTFE was dip-coated on the nickel foam current collector. The mass ratio of Fe_2O_3 and MnO_2 NPs in the slurry was set at approximately 2:1, considering that the specific capacitance of the MnO_2 electrode was larger than twice that of the Fe_2O_3 electrode at entire scan rate range. For this Fe_2O_3/MnO_2 hybrid electrode, it was observed that both ends of the operating voltage were -0.9 V and 0.9 V as shown in Fig. 3(c). The CV shape of the hybrid electrodes indicates that the overall capacitance derives from the combined contribution of the Fe_2O_3 and MnO_2 NPs. Especially, the contribution of Fe_2O_3 seems more dominant in the negative voltage range, while that of MnO_2 does in the positive voltage range. This is also supported by the fact that the CV area in the negative and positive voltage range is proportional to the product of the mass of the Fe_2O_3 and MnO_2 NPs used in the slurry and corresponding C_{sp} value of each electrode, respectively. The C_{sp} value of the hybrid electrode was estimated as lying between the values of Fe_2O_3 and MnO_2 electrode, and reached 198 F/g at the scan rate of 10 mV/s. The voltammetric responses of the Fe_2O_3 single MnO_2 single and Fe_2O_3/MnO_2 hybrid electrodes as a function of the scan rate were shown in Fig. 3(d). For the Fe_2O_3 single electrode, the C_{sp} value of 108 F/g at a scan rate of 10 mV/s dropped to 80.5 F/g at 100 mV/s, and hence the retention was 74.3%. In contrast, for the MnO_2 single electrode, the C_{sp} value decreased from 409 F/g at 10 mV/s to 276 F/g at

100 mV/s, and the retention was 67.5%. In the case of the Fe_2O_3/MnO_2 hybrid electrode, the C_{sp} retention was estimated to be 53.3% at the same scan rate range. The slightly smaller retention of the hybrid electrode indicates that the charge transfer between the dissimilar electrode materials at high scan rates is somewhat slower than that between the same electrode materials. The capacitive properties of the electrodes were also examined by GCD measurements at various current densities, from 2 to 10 A/g. While the single electrodes exhibited gradual potential change during the charge-discharge process, the hybrid electrode showed abrupt increase of the potential at initial stage of the charge process. This is probably due to the different charging rate between the Fe_2O_3 and MnO_2 electrodes.

Although the specific capacitance of the Fe_2O_3/MnO_2 hybrid electrode is lower than that of the MnO_2 single electrode, the extended operating voltage range is expected to enhance the energy density of the device. Fig. 5(a) shows the Ragone plots of the Fe_2O_3 single, MnO_2 single, and Fe_2O_3/MnO_2 hybrid electrodes. The energy density (E, Wh/kg) and power density (P, W/kg) of the electrodes were calculated using the following formulas [31,32],

$$E = \frac{5C_{sp}(\Delta V)^2}{36} \qquad (5)$$

$$P = \frac{3600E}{\Delta t} \qquad (6)$$

where C_{sp} (F/g) is the specific capacitance obtained from the GCD measurements, ΔV (V) is the applied potential window and Δt (s) is the discharge time. It is apparent that the energy density of the Fe_2O_3/MnO_2 hybrid electrode is higher than that of the single electrodes at a given power density, which is reasonably because of the enlarged potential window due to the combined use of two electrode materials.

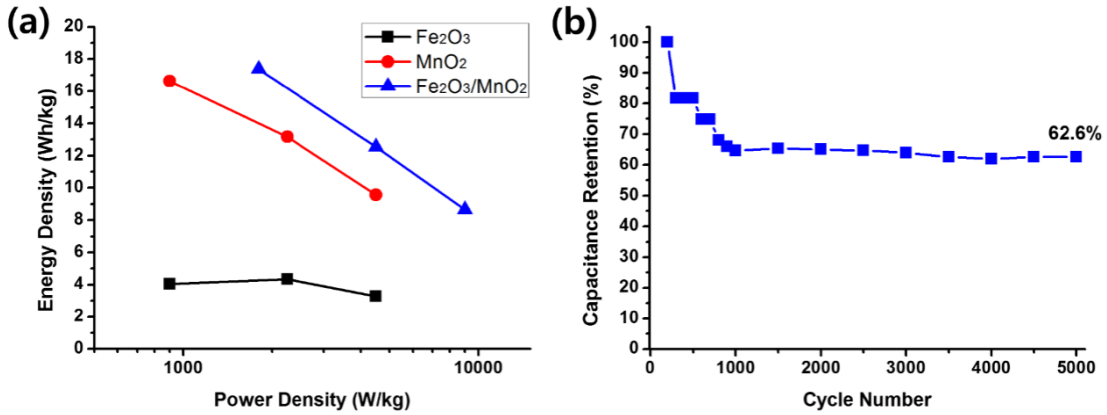

Figure 5. (a) Ragone plots of the Fe_2O_3 single, MnO_2 single and Fe_2O_3/MnO_2 hybrid electrodes. (b) Capacitance retention of the Fe_2O_3/MnO_2 hybrid electrode as a function of the number of galvanostatic charge-discharge cycles at a current density of 10 A/g.

The Fe_2O_3/MnO_2 hybrid electrode exhibited an energy density of 12.5 Wh/kg at a power density of 4500 W/kg. At the similar power density, the Fe_2O_3 and MnO_2 single electrode showed the energy density of 3.3 and 9.6 Wh/kg, respectively. The cycle life of the Fe_2O_3/MnO_2 hybrid electrode

was also examined by continuous GCD cycles at the current density of 10 A/g (Fig. 5b). The C_{sp} of the electrode decreased to approximately 64.6% of the initial value during first 1000 cycles, but remained almost unchanged even after 5000 cycles, indicating the long-term electrochemical stability of the hybrid electrode. Overall, all of the electrochemical performances of the Fe_2O_3/MnO_2 electrode shown in this paper are comparable or somewhat superior to the individual single metal oxide electrode and previously reported hybrid metal-oxide-based electrodes for supercapacitors [20,33-35].

4. CONCLUSION

A hybrid electrode based on Fe_2O_3 and MnO_2 nanoparticles was prepared by dip-coating of the slurry containing two types of nanoparticles on the nickel foam current collector. The Fe_2O_3/MnO_2 hybrid electrode operated stably in the wide voltage range from -0.9 V to 0.9 V, while the Fe_2O_3 and MnO_2 single electrode operated only in the negative and positive voltage range, respectively. In spite that the specific capacitance of the hybrid electrode was lower than that of the MnO_2 single electrode, its energy density was significantly larger than that of the two single electrodes, which is because the extended voltage window contributed more importantly to the enhancement in the energy density of the electrode. The energy density of the hybrid electrode exhibited 12.5 Wh/kg, while that of the Fe_2O_3 and MnO_2 single electrode was 3.3 and 9.6 Wh/kg, respectively, at a power density of 4500 W/kg.

ACKNOWLEDGEMENTS
This work was supported by National Research Foundation of Korea (NRF) Grant (No. 2016R1A5A1012966 and 2017R1A2B4012375) funded by the Korean Government.

References

1. G. Wang, L. Zhang and J. Zhang, *Chem. Soc. Rev.*, 41 (2012) 797.
2. A. Burke, *J. Power Sources*, 91 (2000) 37.
3. P. Simon and Y. Gogotsi, *Nat. Mater.*, 7 (2008) 845.
4. J. Yan, Q. Wang, T. Wei and Z. Fan, *Adv. Energy Mater.*, 4 (2014) 1300816.
5. X. Peng, L. Peng, C. Wu and Y. Xie, *Chem. Soc. Rev.*, 43 (2014) 3303.
6. Y. Zhai, Y. Dou, D. Zhao, P. F. Fulvio, R. T. Mayes and S. Dai, *Adv. Mater.*, 23 (2011) 4828.
7. C. Hu, K. Chang, M. Lin and Y. Wu, *Nano Lett.*, 6 (2006) 2690.
8. J. Zheng, P. Cygan and T. Jow, *J. Electrochem. Soc.*, 142 (1995) 2699.
9. Y. Zeng, M. Yu, Y. Meng, P. Fang, X. Lu and Y. Tong, *Adv. Energy Mater.*, 6 (2016) 1601053.
10. P. Yang, Y. Ding, Z. Lin, Z. Chen, Y. Li, P. Qiang, M. Ebrahimi, W. Mai, C. P. Wong and Z. L. Wang, *Nano Lett.*, 14 (2014) 731.
11. K. Chen and D. Xue, *Sci. Adv. Mater.*, 7 (2015) 2037.
12. Q. Zhang, K. Zhang, D. Xu, G. Yang, H. Huang, F. Nie, C. Liu and S. Yang, *Prog. Mater. Sci.*, 60 (2014) 208.
13. I. Ryu, G. Kim, D. Park and S. Yim, *J. Power Sources*, 297 (2015) 98.
14. I. Ryu, G. Kim, H. Yoon, S. J. Ahn and S. Yim, *RSC Adv.*, 6 (2016) 102814.
15. Y. Yan, B. Li, W. Guo, H. Pang and H. Xue, *J. Power Sources*, 329 (2016) 148.
16. Y. Hu, C. Guan, Q. Ke, Z. F. Yow, C. Cheng and J. Wang, *Chem. Mater.*, 28 (2016) 7296.

17. D. Majumdar, N. Baugh and S. K. Bhattacharya, *Colloids Surf. A Physicochem. Eng. Aspects*, 512 (2017) 158.
18. G. Yu, L. Hu, N. Liu, H. Wang, M. Vosgueritchian, Y. Yang, Y. Cui and Z. Bao, *Nano Lett.*, 11 (2011) 4438.
19. B. Ameri, S. S. H. Davarani, R. Roshani, H. R. Moazami and A. Tadjarodi, *J. Alloys Compd*., 695 (2017) 114.
20. T. Cottineau, M. Toupin, T. Delahaye, T. Brousse and D. Belanger, *Appl. Phys. A*, 82 (2006) 599.
21. R. Liu, J. Duay and S. B. Lee, *Chem. Commun*., 47 (2011) 1384.
22. L. Demarconnay, E. Raymundo-Piñero, F. Béguin, *J. Power Sources*, 196 (2011) 580.
23. J. Yan, Z. Fan, W. Sun, G. Ning, T. Wei, Q. Zhang, R. Zhang, L. Zhi and F. Wei, *Adv. Funct. Mater*., 22 (2012) 2632.
24. X. Zheng, X. Yan, Y. Sun, Y. Yu, G. Zhang, Y. Shen, Q. Liang, Q. Liao and Y. Zhang, *J. Colloid Interf. Sci*., 466 (2016) 291.
25. D. Sarkar, G. G. Khan, A. K. Singh and K. Mandal, *JPCC*, 117 (2013) 15523.
26. A. A. Yadav, *J. Mater. Sci. Mater. Electron*., 27 (2016) 12876.
27. P. Y. Tang, L. J. Han, A. Genc, Y. M. He, X. Zhang, L. Zhang, J. R. Galán-Mascarós, J. R. Morante, J. Arbiol, *Nano Energy*, 22 (2016) 189.
28. S. C. Pang, M. A. Anderson and T. W. Chapman, *J. Electrochem. Soc.*, 147 (2000) 444
29. J. Cao, Y. Wang, Y. Zhou, J. Ouyang, D. Jia and L. Guo, *J. Electroanal. Chem*., 689 (2013) 201.
30. C. D. Lokhande, D. P. Dubal and O. S. Joo, *Appl. Phys*., 11 (2011) 255.
31. V. Khomenko, E. Raymundo-Piñero, F. Béguin, *J. Power Sources*, 153 (2006) 183.
32. T. Brousse, P. Taberna, O. Crosnier, R. Dugas, P. Guillement, Y. Scudeller, Y. Zhou, F. Favier, D. Belanger and P. Simon, *J. Power Sources*, 173 (2007) 633.
33. K. Wang, B. Lv, H. Wu, X. Luo, J. Xu and Z. Geng, *J. Solid State Chem.*, 244 (2016) 75.
34. T. Brousse and D. Belanger, *Electrochem. Solid-State Lett.*, 6 (2003) A244.
35. N. R. Chodankar, D. P. Dubal, G. S. Gund and C. D. Lokhande, *Energy technol.*, 3 (2015) 625.